PCCP

Accepted Manuscript

ROYAL SOCIETY OF CHEMISTRY

www.rsc.org/pccp

Physical Chemistry Chemical Physics
CREATED USING THE RSC LaTeX PCCP ARTICLE TEMPLATE – SEE www.rsc.org/electronicfiles FOR DETAILS
ARTICLE TYPE
www. rsc.org/xxxxxx | XXXXXXXX

Excitation and Quenching Mechanisms in the Near-UV Photodissociation of CH_3Br and CH_3Cl Adsorbed on D_2O or CH_3OH on Cu(110)

E. T. Jensen[a]

Received Xth XXXXXXXXXX 20XX, Accepted Xth XXXXXXXXX 20XX
First published on the web Xth XXXXXXXXXX 200X
DOI: 10.1039/b000000x

Photochemical processes for CH_3X (X=Cl, Br, I) adsorbed on top of thin films of D_2O or CH_3OH on a Cu(110) substrate is studied by time-of-flight mass spectrometry for a range of UV wavelengths (351-193nm). Photodissociation via dissociative electron attachment by photoelectrons and by neutral photodissociation is identified and quantified based on the observed dynamics of the desorbing CH_3 fragments. Photoelectron-driven dissociation of CH_3X is found to be a maximum for monolayer quantities of the D_2O or CH_3OH on Cu(110), but with differing kinetic energy release on the two substrates. The dynamics of CH_3Br and CH_3Cl photodissociation qualitatively differ on CH_3OH/Cu(110) as compared to D_2O/Cu(110), which is ascribed to differing molecular structures for these systems. Evidence is presented for an efficient inter-molecular quenching mechanism for neutral photoexcitation of CH_3Cl and CH_3Br on the CH_3OH/Cu(110) substrate.

1 Introduction

There has been much recent work reported on UV photon- and electron-driven chemical processes in heterogeneous molecular thin films, particularly for water ices. These studies are driven by interests in astrochemistry and planetary science[1–3], as well as terrestrial processes as seen in radiation chemistry[4,5] and photocatalysis[6,7]. A wide range of surface science techniques have been applied to studying these systems. To date there have been relatively few studies of photodissociation dynamics in these types of heterogeneous systems. We have studied a range of halomethanes (CH_3X, X=Cl, Br, I) adsorbed on thin films of D_2O or CH_3OH on Cu(110) substrate. The stimulated dissociation properties of these halomethanes have been studied in some detail in both the gas-phase as well as condensed on surfaces. Depending on the context, these molecules can display low-energy photoelectron driven Dissociative Electron Attachment (DEA) or neutral photodissociation processes when in the adsorbed state.

The solid ices of D_2O and CH_3OH have large bandgaps, with the onset of absorption in solid methanol near 6.7eV ($\lambda < 184nm$)[8], while for water the absorption onset is 8.5eV[9]. However these molecules are known to play roles in electron-driven chemistry in a variety of systems, as the dipolar molecules can solvate low-energy electrons such as photoelectrons[10] or impinging external electrons[11]. The solvation dynamics of electrons at thin water films on metal substrates has been studied extensively by two-photon photoemission[10,12]. Several studies have implicated electron transfer at water-halocarbon interfaces as being responsible for halocarbon dissociation[11,13,14]. Photoelectron dynamics and solvation on CH_3OH[15–17] thin films been studied using two-photon photoemission by a variety of research groups, and is known as a 'hole-getter' when adsorbed on TiO_2[18].

[a] *Department of Physics, University of Northern BC, 3333 University Way, Prince George B.C. Canada V2N 4Z9. Tel: 250-960-6463; E-mail: ejensen@unbc.ca*

The surface chemistry and photochemistry of methyl halides on a variety of metal surfaces has been the subject of many studies[19], as has the adsorption of water[20,21] and methanol[22,23]. There are several previous studies that have looked at the coadsorption systems of methyl halides with water, most particularly chloromethane and water. Due primarily to the electrostatic dipole moments of these species, the interactions between CH_3Cl and D_2O on metals are characterized by repulsion, and has been investigated by temperature programmed desorption (TPD) and modelling studies by Maschoff *et al*[24] who concluded that the long range electrostatic dipole-dipole interactions are an important factor in the CH_3Cl structures. The CH_3Cl binding energies were found to decrease with increasing coverage of D_2O and CH_3Cl, and the repulsive interactions cause CH_3Cl islands to form atop the preadsorbed D_2O or between D_2O islands. Similar conclusions are reached by Lilach and Asscher[25], studying CH_3Cl and H_2O on Ru(100), and inferred the net orientation of the CH_3Cl dipoles from work-function changes during adsorption and TPD. A recent study of CH_3Cl and D_2O on Pd(111) by Fournier *et al* using sum-frequency generation (SFG) spectroscopy[26] concluded that the CH_3Cl adsorbs onto the D_2O through hydrogen bonding between the D and Cl atoms and that the O-D–Cl-CH_3 bonds are aligned close to the surface normal, though with wider angular variation than for Cl–CH_3 on the bare metal surface. Their SFG results also indicate that the large Cl electronegativity induces a partial charge transfer between the surface and the D_2O. There have been several previous studies of photochemistry in these systems– using a UV Hg arc lamp ($h\nu < 5.4eV$) to irradiate CH_3Cl/D_2O/Pt(111), Jo and White[27] highlighted the role of low energy photoelectrons in the observed CH_3Cl photodissociation, and the rapid diminution of the transport of the relevant photoelectrons as the D_2O layer thickness was increased.

There are relatively few previous studies of the dynamics of photodissociation in these heterogeneous systems, in which the mechanisms of photodissociation can be analyzed from the photofragment translational energies. We recently published a study of CH_3I/D_2O/Cu(110) photodissociation at λ=248nm in which the CH_3 photofragment translational energies were analyzed to highlight the varying contributions from neutral photodissociation and photoelectron dissociative electron attachment mechanisms[28]. A study of CH_3I on thick D_2O layers[29] analyzed the ground- and excited state I atoms emitted subsequent to λ=260nm and 290nm photodissociation. These studies showed evidence for a proportion of the I-atoms having larger than gas-phase translational energies which was ascribed to "chattering" during dissociation from 'methyl-down' oriented molecules on the ice surface as well as fast CH_3 photofragments leaving the surface from 'methyl-up' oriented molecules.

1.1 Energetics of Stimulated Dissociation

If one begins by considering the dissociation of a CH_3X molecule in free space, then the requirements of momentum and energy conservation put a limit on how the excess kinetic energy is partitioned between the CH_3 fragment and the halogen atom. For a DEA process the following can be used to rationalize the CH_3 photofragment kinetic energy in terms of

the component energy factors:

$$T_{CH_3} = \frac{m(X)}{m(CH_3X)} \{E_{e^-} + EA(X) - D_0(C-X) + \Delta E_{solv}(X^-) - E_{int}(CH_3)\} \quad (1)$$

where $m()$ is the mass of the particular species, E_{e^-} is the incident electron energy, $EA(X)$ is the electron affinity for the halogen atom X, D_0 is the energy of the bond being broken, $\Delta E_{solv}(X^-)$ is the energy of solvation for the product anion in its dielectric environment and $E_{int}(CH_3)$ is the internal energy (vibration and rotation) of the departing methyl fragment. In principle the solvation energy can be estimated (e.g. Refs.[30,31]) but the uncertainty in various parameters leads to ΔE_{solv} values that have large uncertainty. This is particularly true in the heterogeneous molecular environments of dipolar molecules that we are considering in the present work, in which the solvation energy is structure and site sensitive, and can shift dynamically as the dissociation proceeds. The photoelectron energy E_{e^-} in surface photodissociation is normally taken to be selected from the range of photoelectron energies created by the incident photons at the metal-molecule-vacuum interface[32], and so from the range of photoelectron energies between the Fermi energy E_F and $E_F + h\nu$.

For neutral photodissociation, the analogous equation is:

$$T_{CH_3} = \frac{m(X)}{m(CH_3X)} \{h\nu - D_0(C-X) - E_{int}(X) - E_{int}(CH_3)\} \quad (2)$$

where $h\nu$ is the photon energy, and $E_{int}(X)$ allows for the possible electronic excitation of the departing halogen atom. In surface systems the parent molecule is not in free space, but embedded at or near the vacuuum interface of the system being studied. It is known from prior work in surface photochemistry that the observed fragment kinetic energy distributions can be altered by chemical or post-dissociation interactions, however Eqs. 1 and 2 provide a basis to begin consideration of the observed kinetic energy distributions.

Gas-phase photodissociation of CH_3Br[33,34] and CH_3Cl[35] at λ=193nm occurs in the 'A-band', a set of overlapping excited electronic states. In contrast to the better known case of CH_3I A-band photodissociation, the 193nm photodissociation of CH_3Br and CH_3Cl is dominated by a perpendicular transition from the ground state, mainly via the $^1Q_1$ state, which correlates to dissociation to CH_3 and a ground-state halogen atom. For CH_3Br there is evidence[34] for non-adiabatic coupling with the $^3Q_0$ state, which leads to CH_3 and electronically excited Br^*. Given the experimental geometry used in our work, these neutral photodissociation channels are accessible in the experiments we describe below.

For either A-band neutral photodissociation or photoelectron driven DEA of the halomethanes, the dissociation process is direct, with bond-breaking occurring in a few tens of femtoseconds. Photodissociation of halomethanes adsorbed on or close to a metal surface can be inhibited by quenching[36,37]. When several layers of halomethanes are adsorbed, or are adsorbed on top of a spacer layer of another species, both DEA and neutral photodissociation have been observed. Quenching of one or both photodissociation pathways by the metal surface at these timescales requires a rapid interaction, such as resonant electron/hole transfer between the excited molecule and the substrate[37].

2 Experimental Details

The experiments were performed in an ultra-high vacuum system that has been described previously[38]. The Cu(110) single crystal sample is cooled by liquid nitrogen (base temperature 90K) and can be heated by electron bombardment to 920K for cleaning. Sample cleanliness and order were monitored by Auger electron spectroscopy and low energy electron diffraction measurements respectively.

Neutral products from surface photodissociation travel 185mm to pass through a 4mm diameter aperture to a differentially pumped Extrel quadrupole mass spectrometer (QMS) with an axial electron bombardment ionizer. The sample to ionizer distance is 203mm. Ions created in the ionizer then travel through the quadrupole region and are mass selected, in the present experiments using m/q=15amu. Ion arrivals are recorded using a multichannel scaler that begins counting $50\mu s$ prior to the initiating laser pulse, and the counts recorded from multiple laser pulses are summed. Unless otherwise indicated, the spectra shown in the present work are the result of summing data from 1000 laser pulses into 1000 $1\mu s$ time bins. In order for the ion arrival times to reflect the neutral fragment time-of-flight, they are corrected for the ion flight time (for CH_3^+, $17\mu s$ at the 50eV ion energy used in the QMS). This is the leading systematic uncertainty in the recorded flight times ($\pm 1.5\mu s$) which does not affect comparisons between different TOF spectra but does lead to fixed nonlinear systematic uncertainty in the reported fragment kinetic energies ($KE \propto 1/(TOF)^2$), which is most problematic at short flight times. The TOF spectra $N(t)$ were converted to probability distributions versus CH_3 kinetic energy ($P(E)$) using the Jacobian transformation with a correction factor $1/t$ to account for the reduced ionization probability of faster neutral CH_3 fragments.

The laser pulses (∼5ns duration) are produced by a small excimer laser (MPB PSX-100) operating at 20Hz. In this work 351nm (XeF), 308nm (XeCl), 248nm (KrF) and 193nm (ArF) laser light was used, with laser fluences on the sample of $\sim$ 0.8mJ/cm^2 or less per pulse, depending on the wavelength used. Linearly polarized light has been used exclusively in this work. To create polarized light, the beam passes through a birefringent MgF_2 crystal to separate p- and s-polarized components, which can then be directed at the sample. All of the TOF spectra shown in the present work were obtained using p-polarized light, though we also acquired data using s-polarized light for comparison.† The laser pulses were collimated using a 6mm diameter aperture and were unfocussed on the sample. The laser light is incident upon the sample at a fixed angle of 45° from the mass spectrometer axis– for example, when the Cu(110) sample is oriented to collect desorption fragments along the surface normal direction, the light is incident at 45°.

Deposition of molecules on the sample is done using a microcapillary array directed doser[39], with the sample held normal to the doser, 25mm away. This was found to enhance the deposition by a factor of 10 compared to background dosing. The CH_3Br (Aldrich, ≥99.5%) and CH_3Cl (Aldrich, ≥99.5%) gas used in this work was transferred via a glass and teflon gas-handling system. The CH_3I (Aldrich, 99.5%) dosing used room temperature vapour from the liquid. The D_2O (Aldrich, 99.9 atom % D) and CH_3OH (Aldrich, ≥99.9%) used in this work was degassed by multiple freeze/pump/thaw cycles and

† For work at 248nm and 308nm, s-polarized light was derived from the p-polarized beam by inserting an antireflection coated zero order half-waveplate into the beam. For 193nm and 351nm, s-polarized light was obtained by rotating the MgF_2 crystal to direct the s-polarized beam onto the sample.

was contained in a pyrex vial a few cm from the precision leak valve used to admit gases to the directed doser. The CH_3Br dosing was calibrated by temperature programmed desorption measurements. In this case, 0.95±0.05L CH_3Br was found to correspond to 1.0ML for that substrate. In the present case of adsorption of CH_3Br on D_2O thin films in which the surface structure is less well characterized and no distinct TPD or photochemical signatures define what dose corresponds to monolayer CH_3Br, we report CH_3Br doses in terms of effective monolayers based on this calibration (1.0ML=0.95L). For D_2O we determined an effective monolayer calibration based on findings from TPD and titration of CCl_4 on top of varying D_2O films, which formed atomic chlorine on the metal surface after warming to desorb the molecular layers. From this we found 1.0ML=0.30L for D_2O. A similar procedure was used to calibrate the dosing of CH_3OH, where 0.35L was equivalent to 1ML coverage. In deposition of these molecules, we assumed unit sticking probability on the various substrates for the temperature used for dosing (T<95K).

Details of the adsorption structures found for D_2O/Cu(110) has been the subject of a number of studies, and is summarized in Ref.[21]. Less detail is available on the structure of CH_3OH/Cu(110), though a study using IR spectroscopy[40] indicates that the first layer adsorbs uniformly, and that 3D crystallites grow in the multilayer regime. It is also possible that the D_2O or CH_3OH structures are perturbed by the coadsorption of the dipolar CH_3X molecules[24]. In the results reported in the present work, we have looked for changes in photochemical behaviour as the different molecular coverages were varied, in part as a means to understand what structural changes might be occurring.

3 Results and Discussion

3.1 Photodissociation at 248nm on D_2O/Cu(110)

Time-of-flight spectra at 15amu for CH_3Br adsorbed on D_2O/Cu(110) obtained using 248nm ($h\nu = 5.0eV$) light show two main features, as illustrated in Fig. 1– a photodissociation feature that peaks near $60\mu s$ flight time and a broad, slow photodesorption feature centered around $500\mu s$ flight time. Both of the TOF features are the result of photoelectron transfer from the metal substrate[41] to the CH_3Br layer atop the D_2O layer. This photoelectron driven dissociation and desorption is strongly enhanced as the D_2O coverage is increased to reach one layer of adsorbed D_2O. These features then diminish as the D_2O coverage is further increased, as can be seen in the data of Fig. 2. The overall yields observed for both the photodissociation and photodesorption features are plotted in Fig. 3. The yields reach a pronounced maximum for roughly 1–1.5ML D_2O dosed, and then decrease, roughly exponentially with a 1/e attenuation distance of 2.7ML of D_2O. This attenuation of photoelectron driven dissociation and desorption by ultrathin water layers is consistent with earlier photodissociation findings (1/e=2ML) of Gilton *et al*[42] as well as those of Jo and White[43], who measured an attenuation distance of 2.7ML for D_2O/Pt(111) for photoelectrons above the vacuum level. In the present case it is likely that the photoelectrons responsible for the observed TOF features are subvacuum level "hot" photoelectrons, as discussed below. Although the data of Fig. 3 display a smoothly changing photochemical yield as the D_2O coverage is increased, this does not necessarily mean that the D_2O layer growth is uniform. However the diminution of the photoelectron-driven signal does show that the average

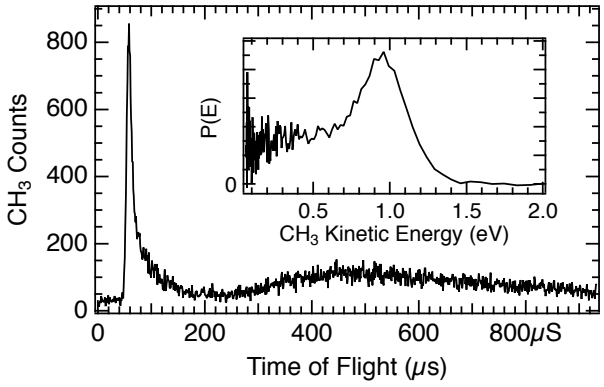

Fig. 1 Time of flight spectrum from the photodissociation of 0.7ML of CH_3Br adsorbed on 1.0ML D_2O/Cu(110) detected at 15 amu (CH_3^+) following 248nm irradiation. The peak at 58μs flight time is due to photodissociation of the CH_3Br and the slower broad peak (500μs) is a result of photodesorption of CH_3Br molecules that dissociate in the mass spectrometer ionizer. The inset plot shows the same data transformed to a probability distribution as a function of CH_3 kinetic energy.

distance from the substrate to the CH_3Br target that is detected in TOF increases with the D_2O coverage.

The photodissociation of CH_3Cl on D_2O/Cu(110) at 248nm has also been studied, with a representative TOF spectrum shown in Fig. 4. The yield of CH_3 photofragments from CH_3Cl on D_2O/Cu(110) is much lower than that seen for CH_3Br, and the spectrum shown is an average of 3 spectra, in order to improve the signal-to-noise ratio. In our experiments we could only detect 248nm photodissociation of CH_3Cl on D_2O/Cu(110) in TOF spectra for a relatively narrow range of D_2O coverages, those close to 1ML which also gave the largest photofragments yields seen for CH_3Br in Fig. 3. For the CH_3Cl/D_2O/Cu(110), the photodesorption feature near 500μs is small relative to that that seen for CH_3Br. Detailed comparison between the 248nm photodissociation of CH_3Cl and CH_3Br on D_2O/Cu(110) is shown in Fig. 5– the CH_3 photofragments from CH_3Cl are roughly 8 to 9μs slower than

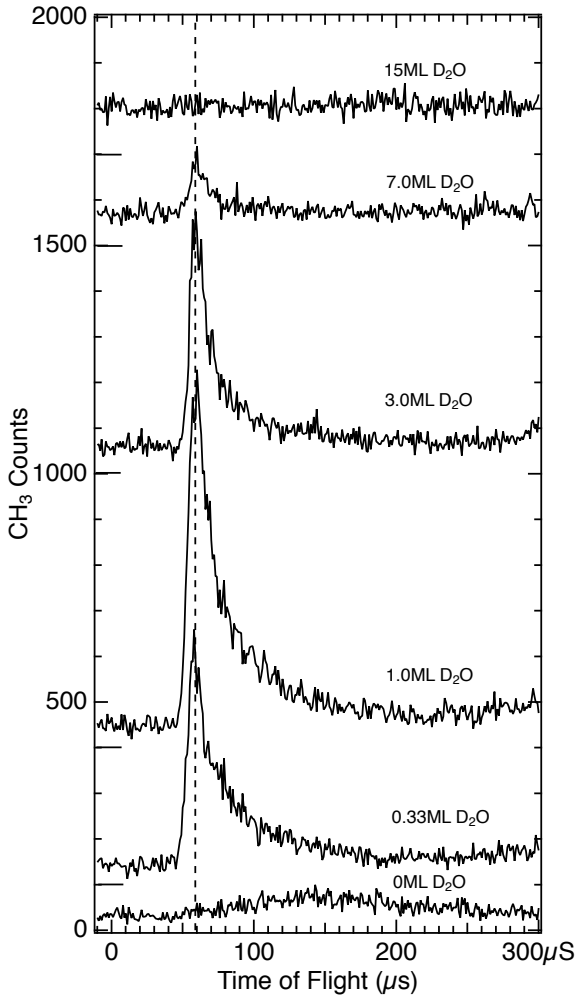

Fig. 2 Sequence of time of flight spectra from 1ML of CH_3Br on D_2O/Cu(110) obtained using varying amount of D_2O and 248nm light. The CH_3Br photodissociation feature at 58μs flight time increases rapidly as the first monolayer of D_2O is added, and then diminishes as the D_2O layer thickness is increased.

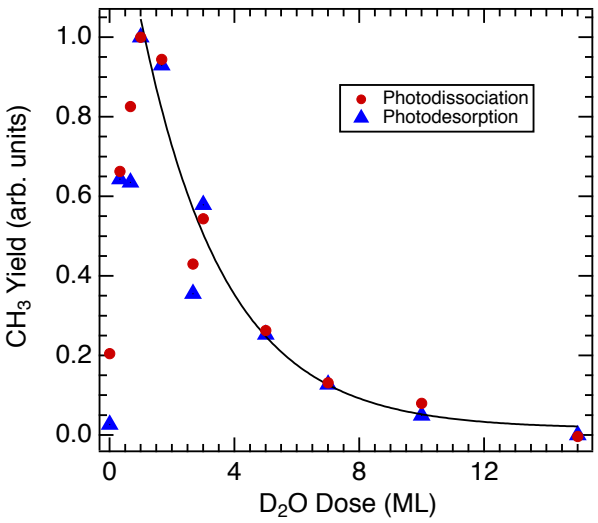

Fig. 3 The yield of CH_3 photofragments obtained from 248nm photodissociation (red circles) and photodesorption (blue triangles) of 1ML CH_3Br on D_2O/Cu(110) as a function of D_2O dose. The solid line represents a simple exponential decay fit to the data points from 1.0ML D_2O and higher- essentially the same fitted function is obtained from either the photodissociation or the photodesorption data.

those from CH_3Br, corresponding to roughly 0.25eV lower translational energy. Based on the free molecule dissociation energetics for DEA from Eq. 1 both the absolute and the relative CH_3 kinetic energies can be considered for the observed photodissociation of CH_3Br and CH_3Cl. The electron affinities of the halogen atoms are 3.36eV (Br) and 3.61eV (Cl), and the dissociation energies D_0 are 3.05eV (CH_3–Br) and 3.63eV (CH_3–Cl)[44‡]. We do not know precise values for the energy contributions from the incident electrons or the anion solvation (E_{e-} and ΔE_{solv} in Eq. 1), but these can be estimated. For CH_3Br condensed in a dielectric medium close to a metal surface, the dissociative anion state is shifted to lower energy[45] and results in a DEA process facilitated by very low energy electrons, close to the vacuum level. Using the estimate for electrons causing DEA of $E_{e-} = 0eV$ (at the system vacuum level E_{vac}) results in ΔE_{solv}=1.06eV for CH_3Br, which is a reasonable value based on estimated values as well as the polarization induced shifts seen experimentally in other similar contexts[46]. It may well be the case that the maximum CH_3Br DEA cross section occurs for electrons below E_{vac}[47,48]. In the case of adsorbed CH_3Cl, it is also well-known that the anion state is shifted to much lower energy relative to the ground-state neutral[45] so that low energy electrons can cause DEA with a large cross section. Assuming E_{e-}=0eV results in an estimate of ΔE_{solv}=1.31eV. This value for ΔE_{solv} appears too large in comparison with that for CH_3Br, since both anions would be expected to be in similar dielectric environments and have similar dissociation times. The value of ΔE_{solv} would be reduced if the relevant E_{e-} for DEA is 0.25eV larger for the CH_3Cl than CH_3Br. This magnitude of differing incident electron energy responsible for DEA is compatible with observations in electron beam experiments on CH_3Cl and CH_3Br condensed on Kr/Pt[45]. While the magnitudes of the polarization shifts are likely different between the Kr/Pt and the D_2O/Cu(110) substrates, the correspondence between the polarization shifts and the requisite incident electron energies seems to be reasonable.

3.2 Photodissociation at 193nm on D_2O/Cu(110)

Irradiation using 193nm ($h\nu = 6.4eV$) light for CH_3Br and CH_3Cl adsorbed on D_2O/Cu(110) produced TOF spectra that display neutral photodissociation of the methyl halides in addition to the photoelectron driven dissociation seen using 248nm light. Figure 6 shows a TOF spectrum for 1ML CH_3Br adsorbed on 1ML D_2O/Cu(110). Although the photon en-

‡ We have used D_0^{298} values without correction for T=90K of our experiment

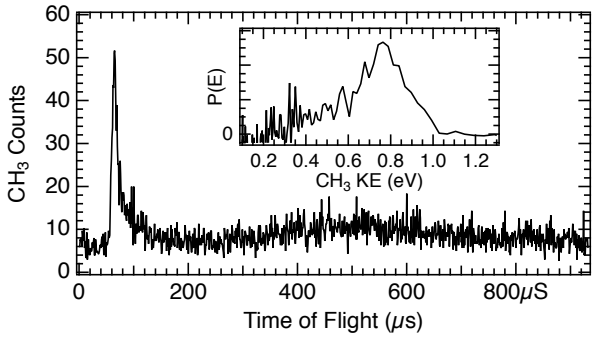

Fig. 4 Time of flight spectrum from the photodissociation of 0.5ML CH_3Cl adsorbed on 1.0ML D_2O/Cu(110) obtained using 248nm light. The spectrum shown is the average of three spectra, in order to improve the signal-to-noise ratio. A photodissociation feature is observed at $65\mu s$ flight time as well as a photodesorption feature centered around $500\mu s$. The inset shows the same data in a CH_3 photofragment kinetic energy distribution, with a peak in $P(E)$ near 0.75eV.

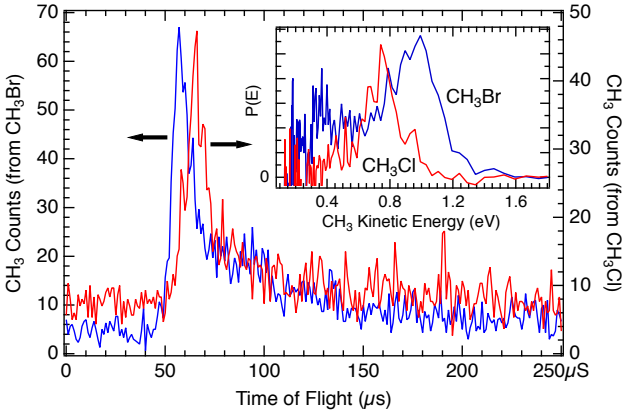

Fig. 5 Comparison of time-of-flight spectra from 0.5ML CH_3Br (blue data) and CH_3Cl (red data) adsorbed on 1.0ML D_2O/Cu(110) obtained using 248nm light. The inset plot shows this data transformed into the CH_3 fragment kinetic energy distributions.

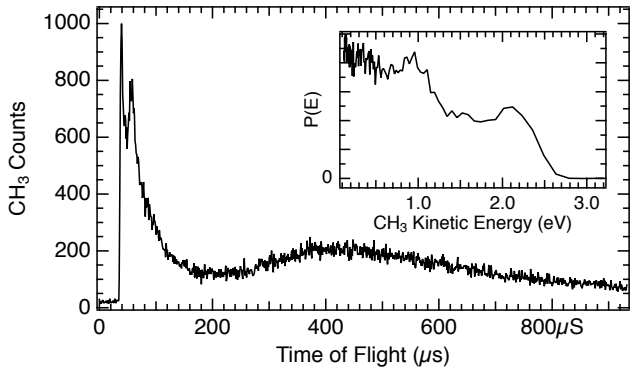

Fig. 6 Time of flight spectrum for 1ML CH_3Br on 1ML D_2O/Cu(110) obtained using 193nm light. As compared to Fig. 1, there is an additional photodissociation component peaking at $38\mu s$ flight time due to neutral photodissociation of the CH_3Br. The inset data shows the distribution of CH_3 photofragment kinetic energies, with the neutral photodissociation peak at 2.1eV and the photoelectron driven DEA feature at 1.0eV.

ergy is 1.4eV larger, so that a wider range of photoelectron energies is generated, the CT-DEA photodissociation feature appears at the same flight time ($60\mu s$) and translational energy (1.0eV) as for the 248nm data. The 193nm photons also produce a neutral photodissociation peak seen at $39\mu s$ flight time, which appears at 2.1eV in the inset photofragment kinetic energy distribution. That the neutral photodissociation is observed for CH_3Br using 193nm light but not for 248nm is consistent with the gas-phase neutral photodissociation cross section, being $6.0 \times 10^{-19} cm^2$ at 193nm, and is at least two order of magnitude smaller at 248nm[49]. Photodissociation TOF features for varying D_2O precoverages are shown in Fig. 7 in which similar variation in the CT-DEA dissociation is seen at 193nm as was the case for 248nm, while the neutral photodissociation feature is seen to increase with the initial D_2O coverage and then remains essentially constant for increasing D_2O layer thickness.

Irradiation of CH_3Cl adsorbed on D_2O/Cu(110) using

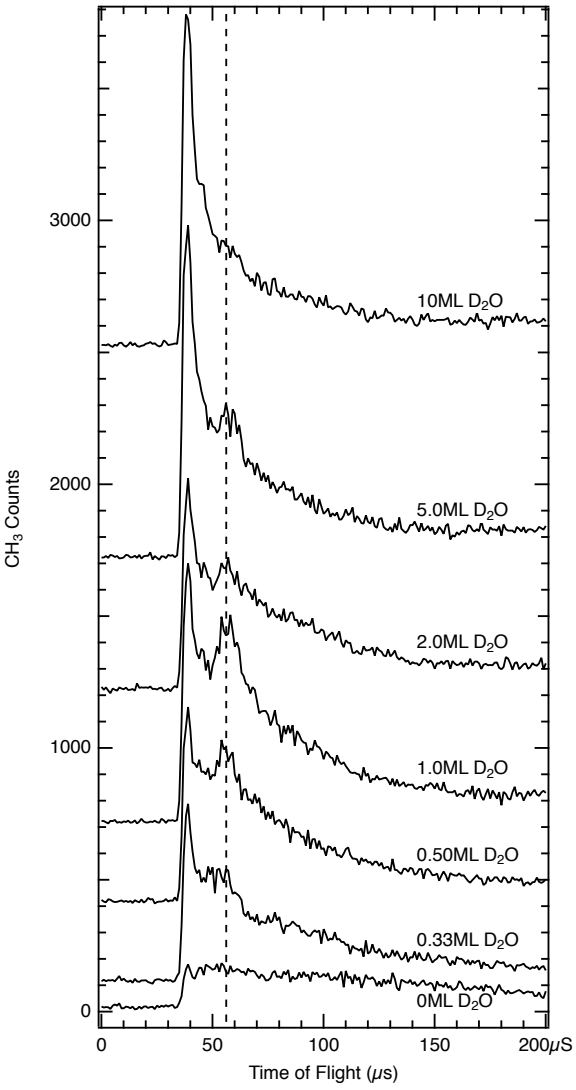

Fig. 7 Sequence of TOF spectra from 1ML CH_3Br on D_2O/Cu(110) obtained using 193nm light for varying amounts of D_2O coverage on the surface. The photoelectron driven photodissociation feature at $58\mu s$ flight time grows rapidly for low D_2O coverages and then diminishes for D_2O layer thicknesses beyond 1ML, while the neutral photodissociation feature at $38\mu s$ grows with D_2O coverage and then remains constant for thicker D_2O layers.

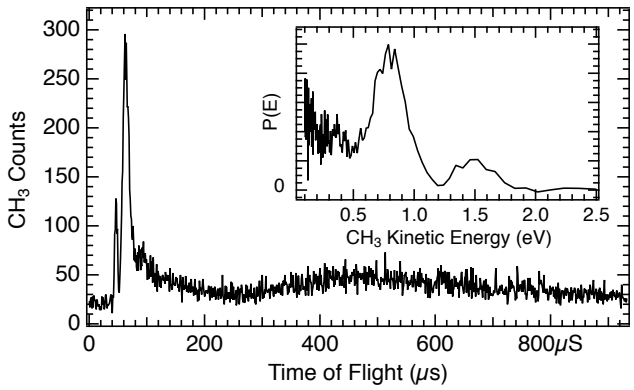

Fig. 8 Time of flight spectrum from 0.7ML CH_3Cl on 1ML D_2O/Cu(110) obtained using 193nm light. As compared to the same system at 248nm (Fig. 4), an additional peak is observed at $46\mu s$ flight time, a consequence of neutral photodissociation. The inset plot shows the data plotted to show the CH_3 kinetic energy distribution, with peaks at 0.8eV (photoelectron DEA) and 1.5eV (neutral photodissociation).

193nm light results in TOF spectra such as that shown in Fig. 8, in which both a neutral photodissociation peak (at $46\mu s$) and a CT-DEA driven dissociation at $62\mu s$ are seen, as well as a small photodesorption feature centered around $500\mu s$. As for CH_3Br, the photoelectron driven photodissociation and photodesorption feature magnitudes are strongly enhanced for roughly 1ML D_2O coverage, and diminish rapidly as the D_2O precoverage is increased above 1ML, as shown in Fig. 9 for the photodissociation peaks. The observation of the neutral photodissociation peak of CH_3Cl at 193nm is reasonable based on the gas-phase cross section of $0.7 \times 10^{-19} cm^2$, which is at least several orders larger than at 248nm[49]. The observed relative yields from neutral photodissociation for CH_3Br and CH_3Cl at 193nm (for example, Figs. 7 and 9) are also consistent with the relative magnitudes ($\sim 9\times$) of the gas-phase cross sections at this wavelength.

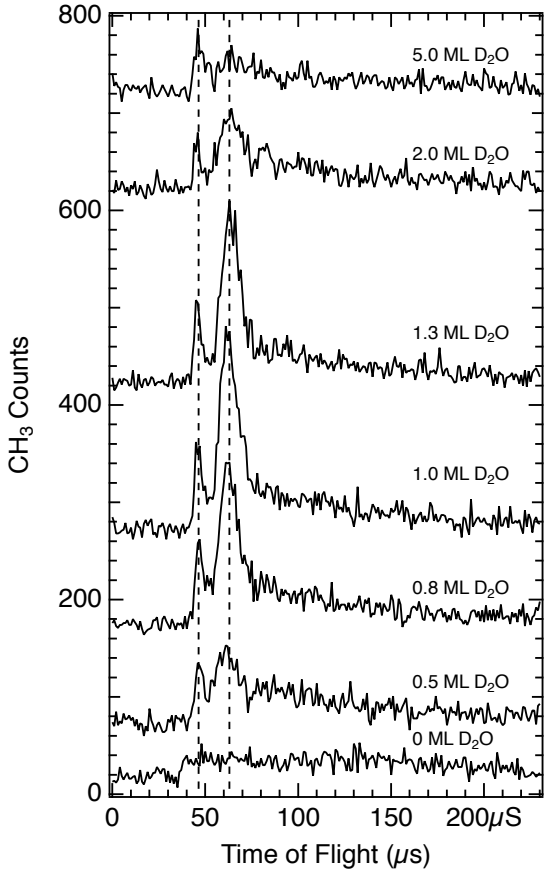

Fig. 9 A sequence of TOF spectra from 0.5ML CH_3Cl adsorbed on varying amounts of D_2O on Cu(110), obtained using 193nm light. The amplitude of the DEA feature is strongly modulated by the D_2O coverage, peaking for 1ML of D_2O. The amplitude of the neutral photodissociation peak is relatively unaffected by the D_2O coverage, beyond a minimum amount.

3.3 Photodissociation at CH_3X on CH_3OH/Cu(110)

As a comparison and contrast to the D_2O/Cu(110) system, we have also studied the photodissociation of the same small halomethane molecules adsorbed on CH_3OH/Cu(110). Methanol has a similar dipole moment[44] (1.70D) to water (1.85D), and on Cu(110) its adsorption results in a comparable decrease in work function ($\Delta\phi$ =-1.35eV for 1ML at 140K[22]) as for water ($\Delta\phi$ =-1.0eV for 1ML[50]). In some respects our photochemical observations from CH_3OH layers are comparable to those from D_2O– the photoelectron-driven DEA processes are strongly enhanced for monolayer coverages and diminish for thicker CH_3OH layers, however the *dynamics* of dissociation are significantly altered. Figure 10 shows comparative TOF spectra for CH_3Br adsorbed on CH_3OH/Cu(110) and D_2O/Cu(110) obtained using 248nm light. For the CH_3OH/Cu(110) substrate, the CH_3Br CT-DEA photodissociation signal is slower, reduced in magnitude and broadened, while the photodesorption signal centered around $500\mu s$ is substantially increased. The inset plot of Fig. 10 highlights the observation that the CH_3 fragments from photoelectron driven dissociation are slower for CH_3Br/CH_3OH than those from CH_3Br on D_2O, with the leading edge of the main TOF peaks separated by $\sim 8\mu s$.

Upon changing the photon energy to 193nm, the TOF spectrum for CH_3Br adsorbed on CH_3OH/Cu(110) of Fig. 11 displays both photoelectron as well as neutral photodissociation features and allows comparison with that from D_2O/Cu(110). The inset plot of the CH_3 fragment kinetic energy distributions shows that the slower CH_3 photofragments seen from CT-DEA of CH_3Br/CH_3OH as compared to CH_3Br/D_2O are unique to the charge-transfer dissociation– the CH_3 photofrag-

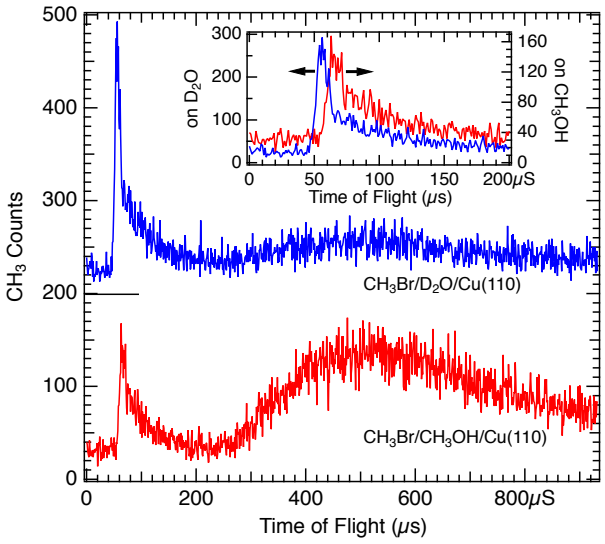

Fig. 10 Comparison of TOF spectra obtained from 0.3ML CH_3Br adsorbed on D_2O/Cu(110) (top, blue trace) with CH_3OH/Cu(110) (lower, red trace), using 248nm light. When adsorbed on CH_3OH (as compared to D_2O), the CH_3Br photodissociation feature near 60μs flight time is reduced in magnitude but broader, whilst the photodesorption feature centered around 500 μs flight time is significantly larger in amplitude. The inset plot shows detail of the CT-DEA photodissociation feature for CH_3Br, being slower on CH_3OH as compared to on D_2O.

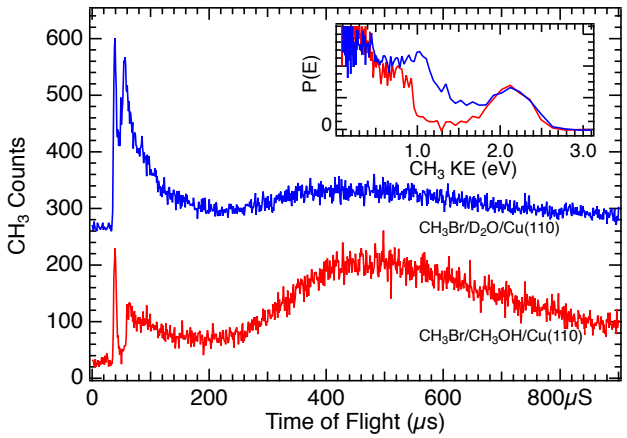

Fig. 11 Comparison of TOF spectra obtained for 0.5ML CH_3Br adsorbed on 1ML D_2O/Cu(110) (top, blue trace) and 1.3ML CH_3Br on CH_3OH/Cu(110) (lower, red trace), using 193nm light. The inset plot shows the same data as a function of the CH_3 fragment kinetic energy. The neutral photodissociation peak (40μs; 2.2eV) is the same on both substrates, while the CT-DEA photodissociation feature is observed to have lower KE on CH_3OH as compared to D_2O, as also seen at 248nm in Fig. 10.

ments from neutral photodissociation at 193nm have the same translational energy on both molecular films.

Figure 12 highlights another difference seen for CH_3Br adsorbed on CH_3OH/Cu(110)– though using 193nm light has a photon energy sufficient for neutral photodissociation of CH_3Br, this is not observed at low coverages of CH_3Br on CH_3OH and is seen only for CH_3Br coverages beyond roughly 1ML, independent of the precoverage amount of CH_3OH. This is in contrast to the analogous situation seen for D_2O/Cu(110), in which the 193nm neutral photodissociation is not observed to have a minimum onset coverage of CH_3Br.

Based on the findings for CH_3Br on CH_3OH/Cu(110), the expectations for CH_3Cl adsorbed on this substrate would be for a reduced but broadened photoelectron-driven dissociation signal and increased photodesorption. In this light, the observed TOF spectra for this system, such as that of Fig.

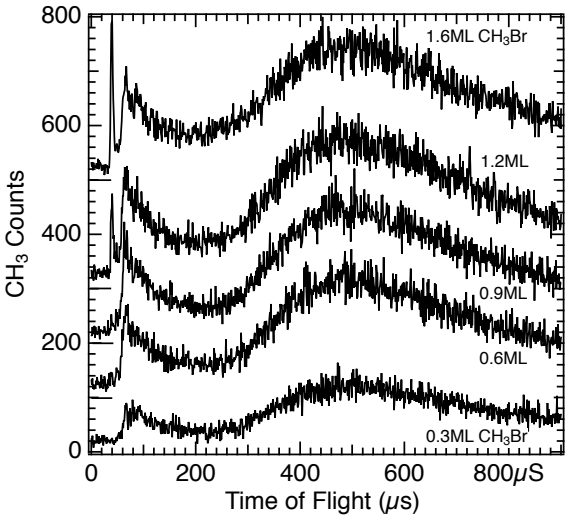

Fig. 12 A series of TOF spectra for varying amounts of CH_3Br adsorbed on 1ML CH_3OH on Cu(110), obtained using 193nm light. While the CT-DEA photodissociation and the photodesorption features are observed at all CH_3Br coverages, the neutral photodissociation of CH_3Br is only observed for coverages of CH_3Br above 1ML.

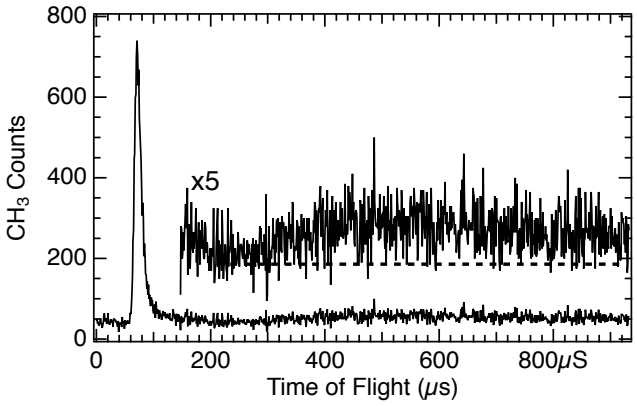

Fig. 13 Time of flight spectrum from the photodissociation of 0.3ML CH_3Cl adsorbed on 1ML CH_3OH/Cu(110) using 248nm light. The photodissociation via the DEA mechanism give a large yield of CH_3 photofragments (peak at $71\mu s$), and a very small photodesorption feature (the dashed line indicates the CH_3 background count level).

13 are surprising. The yield of CH_3 photofragments from photoelectron-driven dissociation is very large and also narrow in the TOF spectra compared to the analogous case for CH_3Br, and the photodesorption feature is much smaller than that seen in the previously described systems. In common with the findings for CH_3Br, the CT-DEA photodissociation peak for CH_3Cl on CH_3OH/Cu(110) is at a longer flight time than seen for D_2O/Cu(110), as shown in Fig. 14. As compared to the D_2O case, the CH_3 photofragments from CH_3Cl photodissociation are $\sim 6\mu s$ slower, or as shown in the inset plot of Fig. 14, the peak in the $P(E)$ distribution is at 0.15eV lower kinetic energy.

That the observed photodissociation for CH_3Cl on CH_3OH/Cu(110) is photoelectron driven is supported by data such as that shown in Fig. 15, in which the amount of CH_3OH is varied for a fixed CH_3Cl dose. The photodissociation yield

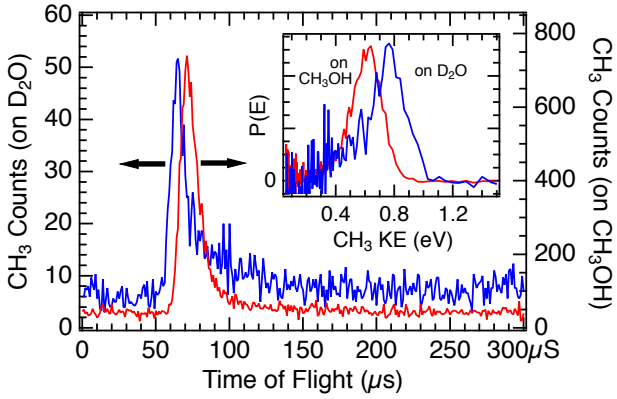

Fig. 14 Comparison of TOF spectra for CH_3Cl photodissociation at 248nm, between that adsorbed on D_2O/Cu(110) (blue trace) and on CH_3OH/Cu(110) (red trace). The inset plot shows the same data plotting the probability distribution as a function of the CH_3 photofragment kinetic energy. While the yield of CH_3 photofragments is much larger for CH_3Cl adsorbed on CH_3OH (note the respective y-axis scales for the TOF spectra), the kinetic energy release is smaller than when adsorbed on D_2O/Cu(110).

is found to increase dramatically from that of the clean surface, to a maximum yield found for roughly 1ML CH_3OH. The yield is then observed to decrease, and a simple exponential fit suggests an attenuation length of 3.0ML for the relevant photoelectron transport through CH_3OH, which is comparable to the 2.7ML discussed above for D_2O. Similar variations with CH_3OH dose are also found for CH_3Br/CH_3OH for the photoelectron driven photodissociation peak as well as for the photodesorption feature. The neutral photodissociation peak for CH_3Br seen at 193nm (the TOF peak at $39\mu s$ in Fig. 12) behaves differently– increasing monotonically with for low CH_3OH doses and remaining essentially constant for higher multilayer doses. As the CH_3Cl coverage is increased for a fixed amount (1ML) of CH_3OH, the CH_3 photoyield due to photoelectron driven dissociation grows monatonically with the CH_3Cl dose until 1ML is dosed, and then remain essentially fixed for higher doses. We interpret this result as being due to having only the first monolayer of CH_3Cl able to stick to the CH_3OH/Cu(110) substrate at the temperature used for our experiments.

It is also notable that the CH_3 photofragment translational energy distribution from DEA does not change as the CH_3OH thickness is varied nor over the range of wavelengths that CH_3Cl/CH_3OH/Cu(110) photodissociation is observed (308nm to 193nm)– TOF spectra from different wavelengths can be overlaid and aside from simple linear scaling, are otherwise identical. This also appears to be the case in our data for the CH_3Br on D_2O/Cu(110) and CH_3OH/Cu(110), though the distributions are more complex. This point is salient as photodissociation via DEA is often interpreted in terms of the '3-step model' [32,51] in which the energy available for dissociation should reflect the convolution of the photoelectron distribution with the anion resonance attachment energy distribution. This leads to an expectation for lower energy available (Eq. 1) at the red end of the wavelengths used for photodissociation that should be reflected as a suppression of the high-energy side CH_3 translational energy distributions, but this is not observed. One possible explanation for this lack of correlation between photon energy and fragment translational energy could be that intermediate electron sates modify the density of states at the vacuum interface, such as image-potential derived states [15] that couple with the anion attachment resonance [52].

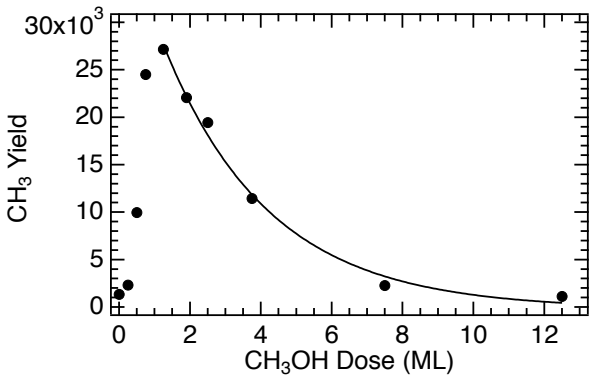

Fig. 15 Yield of CH_3 photofragments from photodissociation of CH_3Cl/CH_3OH/Cu(110) as the CH_3OH coverage is varied. The data is obtained using 193nm light and 1ML of CH_3Cl. The solid line is a simple exponential fit to the data points above 1ML CH_3OH coverage, and represents a 1/e attenuation distance of 3.0ML for CH_3OH.

A striking observation for CH_3Cl/CH_3OH/Cu(110) at 193nm is that we do not observe CH_3 photofragments from neutral photodissociation of the CH_3Cl at 193nm under any of the conditions studied– data obtained at 193nm is essentially identical to that from 248nm as shown in Fig. 13. Given the cross sections and intensities measured for CH_3Cl/D_2O/Cu(110) (e.g. Fig. 9), the neutral photodisso-

ciation channel should be easily observable. The absence of neutral photodissociation in the TOF spectra from the first monolayer of CH_3Br on CH_3OH/Cu(110) that is seen in Fig. 12 indicates that the neutral photodissociation mechanism is suppressed at 193nm for CH_3Cl and CH_3Br on the CH_3OH/Cu(110) substrate. This observation is discussed further in Section 4.

As described above, we see altered kinetic energy distributions for the CH_3 photofragments via CT-DEA for CH_3X on CH_3OH as compared to D_2O. We have also directly compared the observed distributions for CH_3Cl to those of CH_3Br adsorbed on CH_3OH, which are shown in Fig. 16 for 248nm light. The CH_3 photofragments from CT-DEA of CH_3Br are slightly faster than those from CH_3Cl in the onset of the distribution as well as the most probable time. As shown in the inset plot, the leading edge of the $P(E)$ distribution is at 0.20eV higher energy for the CH_3Br as compared to that of CH_3Cl. This is a smaller kinetic energy difference than was seen for these two molecules on D_2O in Fig. 5 ($\sim$0.3eV). This smaller difference in kinetic energies is a result of the larger downward shift in CH_3 fragment kinetic energy for CH_3Br on CH_3OH as compared to D_2O ($\Delta T_{CH_3} = -0.20eV$) as compared to that for CH_3Cl ($\Delta T_{CH_3} = -0.15eV$).

3.4 Cross Sections

We have measured depletion cross sections for a selection of the molecular thin films examined in this work. These cross sections are obtained by recording CH_3 photofragment yields from photodissociation and/or photodesorption for a sequence of TOF spectra. Time-of-flight spectra are obtained using 200–300 laser pulses per scan, then repeated for 10 or more

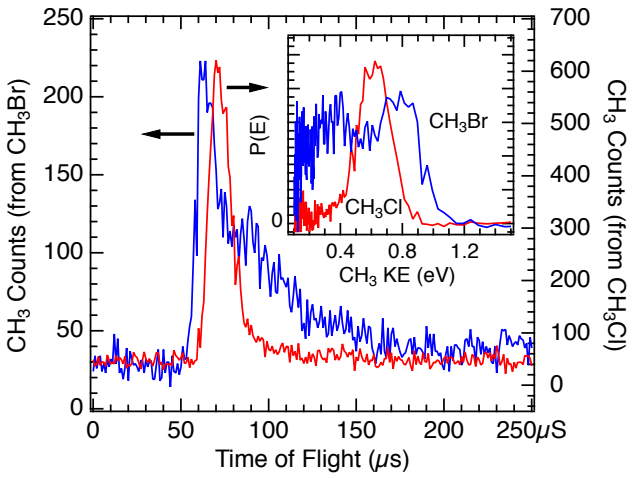

Fig. 16 Comparison of the 248nm photodissociation of CH_3Br (blue trace) and CH_3Cl (red trace) adsorbed on 1ML CH_3OH/Cu(110). The inset plot shows the related probability distributions as a function of the CH_3 fragment translational energy.

successive scans. In the systems studied here, the TOF signals are observed to diminish as the net laser photon flux was increased, and the resulting yield vs flux curves could be fit by a simple exponential decay model. Reasonable fits to the data were obtained, at least in the low flux limit, though this does not exclude the possibility that more complex photochemical processes not seen in the TOF data might be occurring in these heterogeneous thin films. In the cases where multiple features are observed in the TOF spectra (neutral photodissociation, DEA, photodesorption) we measured separate depletion cross sections for each feature. In the cases we examined, we measured the same (within experimental error) cross sections for co-present features. The resulting extracted cross sections are reported in Table 1. The values reported are nearly all obtained using 1ML of the D_2O or CH_3OH, with between 0.5 and 1ML of the methyl halide adsorbed on top. The one exception is for the λ=193nm photodissociation of CH_3Br/D_2O in which we also report the value for 15ML of D_2O (value

in brackets) which represents the cross section in which only neutral photodissociation is observed in the TOF spectra. This value of 9.2×10^{-19}cm^2 is somewhat larger than that reported for gas-phase[49] CH_3Br ($\sigma = 6 \times 10^{-19}$cm^2). This discrepancy may well be due to the rather large error associated with the absolute cross sections we estimate ($\pm 50\%$)[§]. In several cases we can observe and identify the photochemical processes in the TOF spectra (and some of these are shown and discussed above) but the yields are too low to yield a reliable cross section estimate, so these are denoted by '>0'. Situations in which no photochemical signals could be discerned in the TOF spectra are denoted by '-'. The tabulated values highlight an interesting contrast between the CH_3Br and CH_3Cl photodissociation results- the CH_3Br photodissociation is observed at longer wavelengths on the D_2O/Cu(110) films, while for CH_3Cl, the photodissociation is larger and seen at longer wavelengths on the CH_3OH/Cu(110) films. We are not aware of any previous observations of CH_3Cl photodissociation with substantial cross section for λ =308nm (4.02eV) photons. There are few previously reported photochemical cross-sections for halomethanes co-adsorbed with D_2O or CH_3OH. A study of CD_3Cl caged within H_2O layers on Ru(100) measured cross sections of $\sim 0.5 \times 10^{-18} cm^2$ at 193nm and $\sim 0.02 \times 10^{-18} cm^2$ at 248nm by observation of CD_3Cl depletion[53], values that are compatible with those reported for CH_3Cl/D_2O/Cu(110) in Table 1.

§ Various geometrical factors as well as the variable laser beam profile uniformity lead to this large absolute error. At a given wavelength, the *relative* errors of our cross section estimates are quite small– we typically measured cross sections for different molecular combinations on the same day without modifying the laser geometry and using the same laser gas fill, so that the sources of most relative errors are small (<10%) for these values. We do expect that our absolute cross section values and those for comparing values at two different wavelengths have larger errors.

3.5 Angular Distributions

The substantive differences observed in the photodissociation dynamics between CH_3Br and CH_3Cl when adsorbed on CH_3OH/Cu(110) were further investigated by measurements of the angular variation of the signals. For CH_3Cl/CH_3OH/Cu(110) we found an angular distribution for the CH_3 photofragments well fit by a $\cos^N\theta$ functional form with $N = 4$, which does not change substantially with CH_3Cl coverage. As the detection angle from the surface normal increases, the CH_3 photofragment kinetic energy distribution is hardly affected, as seen in Fig. 17. There is a small diminution of the fastest CH_3 fragments at larger escape angles, but no increase in the proportion of the lower energy inelastic tail even for the 60° detection angle. In contrast, the TOF spectra for CH_3Br photodissociation (e.g. Fig. 11) show clear evidence of inelastic interactions on both the D_2O/Cu(110) and CH_3OH/Cu(110) surfaces. The $P(E)$ distributions for a range of detection angles shown in Fig. 18 for CH_3Br/D_2O/Cu(110) display a more pronounced inelastic tail for CH_3 kinetic energies lower than that of the main CT-DEA peak, and in some spectra a peak can be discerned near $T_{CH_3} \approx 0.4$eV (e.g. insets in Figs. 5 and 16). We ascribed a similar feature seen for CH_3I/D_2O/Cu(110) to chattering as downward pointing CH_3 fragments interact with the substrate before escaping[28]. The inelastic signals are seen to grow in relative size as the detection angle from the surface normal is increased. The angular distributions of the CH_3 photofragments from CH_3Br are peaked in the surface normal direction ($\propto cos^N(\theta)$ with N=4–5) but also display a shift to lower kinetic energy in both the fastest CH_3 photofragments as well as the larger 'inelastic tail' as the angle increases.

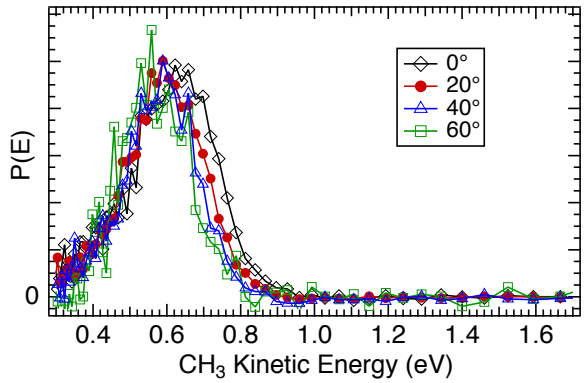

Fig. 17 Comparison of the CH_3 photofragment translational kinetic energy distributions from 248nm photodissociation of CH_3Cl adsorbed on 1ML CH_3OH/Cu(110) as a function of detection angle from the surface normal.

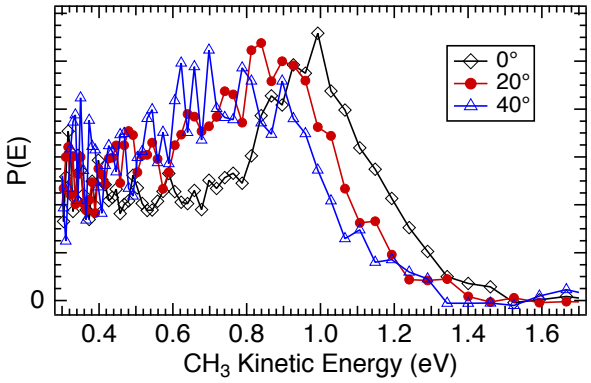

Fig. 18 Comparison of the CH_3 photofragment probability distributions from 248nm photodissociation of CH_3Br adsorbed on 1ML D_2O/Cu(110) as a function of detection angle from the surface normal.

4 Additional Discussion

4.1 Structure and Dynamics

In many respects the structural properties of the halomethanes are quite similar, with the structure of the solids dominated by the electrostatic dipole interactions (dipole moments: CH_3Cl- 1.90D; CH_3Br- 1.82D; CH_3I- 1.64D)[44]. In the bulk solid, although the molecular ordering is dominated by dipolar interactions, there are distinct differences between the structure of crystalline CH_3Cl[54] and CH_3Br[55], which is ascribed to differences in the halogen-halogen binding interactions[55]. The observed photochemical dynamics for CH_3Br and CH_3Cl on D_2O/Cu(110) do not indicate significant differences in the structural aspects that impact the observed dynamics. For both methyl halides, we observe CT-DEA on thin D_2O films over a range of wavelengths in which hot photoelectrons of the appropriate energies would be generated. In addition we observe photodesorption of the intact CH_3X molecules that correlate with the CT-DEA dissociation fluxes. The observed dynamics are compatible with an antiferroelectric structure for the methyl halides, and given the net repulsive interactions with the D_2O, it is anticipated that CH_3X islands are present even at low coverages. These observations are consistent with our previous study of CH_3I/D_2O/Cu(110)[28]. At the shorter 193nm wavelength, we also observe neutral photodissociation of both CH_3Br and CH_3Cl, with apparent cross sections comparable to those for the gas-phase. That these neutral photodissociation TOF features are very well-defined indicates that the measured CH_3 photofragments are from 'CH_3-up' oriented molecules that do not significantly interact with the surface during or post bond-cleavage.

The clean Cu(110) substrate has a work function of 4.48eV[44], and the D_2O and CH_3OH adlayers reduce the work function by 1eV or more for monolayer coverages[22,50]. In addition, the CH_3X adlayers are known to reduce the work function on D_2O[25,26] due to the preferred orientation of the dipole. Hence even for the longest wavelength (351nm, hν=3.51eV) used in this work, we expect that free photoelectrons (i.e. above the vacuum level) are present under most conditions studied, in addition to the subvacuum level 'hot' photoelectrons. At λ=351nm we only observed photoelectron-driven dissociation and photodesorption in the TOF spectra for the $CH_3Br/D_2O/Cu(110)$ and $CH_3I/D_2O/Cu(110)$ systems. Photodissociation was observed for a narrow range of D_2O coverages around 1ML, where the work function minimum and maximum CH_3 yields (e.g. Fig. 3) are found. Since we observe no photoelectron-driven dissociation of CH_3Cl on either $D_2O/Cu(110)$ or $CH_3OH/Cu(110)$ using 351nm light, it can be concluded that higher energy photoelectrons are required for DEA of CH_3Cl than are substantially available. Upon increasing the photon energy by 0.49eV using 308nm light (and consequently producing a similarly increased range of photoelectron energies), we observe not only much stronger dissociation signals from $CH_3Br/D_2O/Cu(110)$ but also photodissociation of $CH_3Cl/CH_3OH/Cu(110)$. This indicates a threshold photon energy between 3.53eV and 4.02eV for the latter system. The contrasting behaviour of CH_3Br and CH_3Cl photodissociation yields on $D_2O/Cu(110)$ and $CH_3OH/Cu(110)$ are highlighted near these thresholds. The CT-DEA photodissociation of CH_3Cl is most prominent on the $CH_3OH/Cu(110)$ surface, and is only observed at shorter wavelengths on $D_2O/Cu(110)$ and with lower CH_3 photofragment yields and cross-section. In contrast the CH_3Br CT-DEA photodissociation is more prominent on the $D_2O/Cu(110)$, and we did not observe CH_3 photofragments or photodesorption on $CH_3OH/Cu(110)$ using 351nm light. We believe that these observations are related to the differing molecular structures of CH_3Br and CH_3Cl on the CH_3OH and D_2O molecular interfaces.

Further evidence for differing molecular ordering of CH_3Br and CH_3Cl on the two substrates considered comes from the observed CH_3 time-of-flight distributions. The TOF spectra from $CH_3Cl/CH_3OH/Cu(110)$ display a single narrow features due to CT-DEA of the CH_3Cl ($\overline{E}$=0.62eV, ΔE=0.24eV FWHM). This system displays almost no 'inelastic tail' of lower energy CH_3 photofragments (E_{trans} <0.4eV, see Figs. 16 and 17) and there is only a very small photodesorption feature as compared to the other systems studied in this work. These observations for $CH_3Cl/CH_3OH/Cu(110)$ lead us to propose that the CH_3Cl molecules are adsorbed primarily with the Cl–CH_3 axis normal to the surface and in the 'CH_3-up' orientation. Bond-breaking due to DEA leads to the departing CH_3 photofragment having little opportunity for inelastic interactions as it departs the surface and hence a relatively narrow translational energy distribution. Due to the solvation shift of the anion, the dissociation probability is high (i.e. low autoionization or quenching probability) so there is a relatively low probability for excited CH_3Cl that do not dissociate but might have sufficient energy to break the molecule-surface bond and contribute to photodesorption. On the $D_2O/Cu(110)$ surface the photodissociation of CH_3Cl yields fewer CH_3 photofragments and a significantly lower cross section (Table 1). The data such as in Figs. 4, 8 and 14 show that there is a similarly small inelastic tail ($E_{trans} < 0.5$eV) and

a somewhat larger photodesorption signal as compared to the situation on CH_3OH/Cu(110). An IR-SFG study of CH_3Cl on D_2O/Pd(111) indicates that the Cl–CH_3 bond is along the surface normal in the 'CH_3-up' orientation[26], and our own observations of the angular distributions for CH_3 photofragments on both CH_3OH and D_2O are in accord with this. Depending on the dosing order and amount[25], it is possible that some mixed orientations for CH_3Cl on D_2O can be formed. We do believe that the CH_3Cl/D_2O/Cu(110) TOF data shows evidence for a minor amount antiferroelectric ordering of the CH_3Cl– that downward pointing CH_3 photofragments will inelastically scatter from the surface to contribute to the inelastic tail, and that 'chattering' type interactions will also lead to more quenching and subsequent molecular photodesorption[56] on D_2O/Cu(110) than for CH_3OH/Cu(110).

On the basis of the observed energy and angular distributions, we conclude that CH_3Br on the D_2O/Cu(110) and CH_3OH/Cu(110) substrates has a mored mixed orientational ordering than for CH_3Cl, most likely an antiferroelectric structure with both 'Br-up' and 'Br-down' configurations, though to a lesser extent on D_2O/Cu(110) than for CH_3OH/Cu(110). The role of local work function modulated by the ordering of surface dipoles at the interface has been noted previously[47,57], and in the case of CH_3OH/Cu(110), the preponderance of 'CH_3–up' ordering of the CH_3Cl lowers the barrier for photoelectron interactions to a larger extent than the mixed ordering of the CH_3Br. In an analysis of CH_3Br electron- and photodissociation on Ru surfaces it was found that the 'Br-down' configuration largely results in photodissociation while the 'Br-up' configuration leads to photodesorption[56]. We also see that there are differences in the solvation of CH_3Br and CH_3Cl anion states on the two substrates considered, as both are found to have lower CH_3 kinetic energies on CH_3OH/Cu(110) but with a larger downward energy shift for CH_3Br. Based on Eq. 1 this indicates that the dissociating CH_3Br anion is less well solvated than CH_3Cl on the CH_3OH, which could be due to differences in the orientational structure as discussed above, or could be due to steric hindrance for the larger neutral CH_3Br precursor.

There has been less previous work for the CH_3OH thin films, but FT-IR spectroscopy indicates that the equilibrium structure for CH_3OH/Cu(110) at low temperatures has the O–H group close to parallel to the surface, with the CH_3 group oriented toward the surface normal[40]. This is responsible for the sign and magnitude of the surface dipole and the related change in work function that has been observed. This surface dipole structure would most likely cause the preferential orientation of the halomethanes in a similar manner as for the D_2O/Cu(110) case.

4.2 Neutral Photodissociation and Quenching

The neutral photodissociation of CH_3Br and CH_3Cl in the gas-phase at 193nm has been well-studied[33–35] and occurs with rapid C–X bond scission via a set of excited states referred to as the 'A-band'. In many respects this photodissociation is similar to that of CH_3I at 248nm, and we recently reported[28] on the 248nm photodissociation of CH_3I/D_2O/Cu(110) in which neutral photodissociation was prominent, and was identifiable for D_2O films from monolayer to many multilayers in thickness. For both CH_3Br and CH_3Cl on D_2O/Cu(110) we do identify the neutral photodissociation pathway using λ=193nm light from the characteristic CH_3 kinetic en-

ergy distributions. When these molecules are adsorbed on CH_3OH/Cu(110) however the situation is dramatically different. We do not observe neutral photodissociation of CH_3Cl, and neutral photodissociation of CH_3Br is not observed for submonolayer CH_3Br coverages. We have also examined the 248nm photodissociation of CH_3I/CH_3OH/Cu(110) over a range of conditions (e.g. Fig. 19) and do indeed observe characteristic TOF features that can only be a consequence of neutral photodissociation. While in many other respects the behaviour of CH_3I on CH_3OH/Cu(110) was found to be similar to that of CH_3Br, the quenching of neutral photodissociation seen for CH_3Br and CH_3Cl at 193nm is absent for the CH_3I at 248nm. In the absence of any detailed calculations for the ground and excited state energy levels of the CH_3X/CH_3OH/Cu(110) system, it is difficult to pin down the precise mechanism by which the excitations are quenched. We can exclude mechanisms such as orientational or steric blocking on the basis of the observed CT-DEA dissociation dynamics of the CH_3X on the same substrate, which is not similarly hindered. It is apparent that an efficient quenching due to a Dexter energy transfer (DET) mechanism is present for CH_3Br and CH_3Cl using 193nm photoexcitation.

Solid methanol has a bandgap of 6.7eV, and UPS study of CH_3OH/Cu(110)[22] places the HOMO $2a''$ level 5.5eV below E_F, while for H_2O/Cu(110) the HOMO $1b_1$ level is located 6.8–7.2eV below E_F[20]. As for the methyl halides, a study of CH_3X/Ag(111) using UPS placed the halomethane HOMO at 6.0eV below E_F for CH_3Cl/Ag(111), and at 5.4eV and 4.4eV respectively for CH_3Br and CH_3I monolayers on the same substrate[58]. The other ingredient required for DET is wavefunction overlap, and based on isolated molecule wavefunctions the HOMO of CH_3OH has more weight on the CH_3 group than the $1b_1$ level of D_2O does on its free D, and so is consistent with this requirement. It is of note that in CH_3OH/TiO_2 photochemistry, it has been remarked in several studies[18,59] that the CH_3OH is an effective 'hole getter' as compared to H_2O/TiO_2. This is attractive explanation since the neutral excited state and the DEA anion state both correspond to an excess electron in the CH_3X LUMO, so the differences between these two dissociative processes are largely restricted to the differences in time that the excited state lies above the corresponding ground state prior to curve-crossing and the presence of the valence hole for the neutral excitation. However it is unclear if the quenching of the excited state hole for CH_3X by CH_3OH can be rapid enough to compete with the very rapid bond scission in CH_3X A-band photodissociation. We are not aware of similar inter-molecular quenching of rapidly dissociative neutral photoexcitation having been previously identified in the surface photochemistry literature. A somewhat similar quenching mechanism has been identified in X-ray absorption studies of homomolecular clusters of CH_3Br[60], although in this case the $3d \rightarrow 4a_1$ core-valence ex-

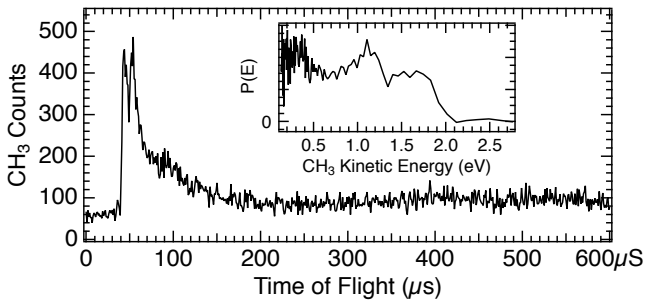

Fig. 19 Time of flight spectrum for CH_3 photofragments from 1 ML of CH_3I adsorbed on a thick (≈10ML) film of CH_3OH on Cu(110) obtained using 248nm light. The prominent peaks at $44\mu s$ and $54\mu s$ flight times are characteristic of the neutral photodissociation pathways for CH_3I in the A-band.

citation has dissociation competing with Auger decay, and the quenching observed in clusters is ascribed to delocalization of the CH_3Br LUMO, rather than the HOMO implicated in the present work.

5 Acknowledgements

The author thanks G.D. Muirhead, C. Miller and E. Schibli, who provided assistance with the experiments as a part of their NSERC Undergraduate Student Research Award tenures in the laboratory. The Natural Sciences and Engineering Research Council (NSERC) of Canada is acknowledged for financial support of this work.

Table 1 Observed depletion cross sections based on observed photodissociation and photodesorption yields from CH_3X on different monolayer films on Cu(110), and gas-phase photodissociation cross section[49]. Entries indicated by '>0' have detectable yields but insufficient signal to measure a reliable cross section. Entries indicated by a dash '-' had no detectable photochemical signal in the TOF spectra. The value in brackets for CH_3Br/D_2O at 193nm is that from a multilayer D_2O film

	Depletion Cross Section ($\times 10^{-18} cm^2$)					
λ (nm) [$h\nu$(eV)]	CH_3Br/D_2O	CH_3Br/CH_3OH	CH_3Cl/D_2O	CH_3Cl/CH_3OH	CH_3Br(gas)[49]	CH_3Cl(gas)[49]
193 [6.42]	1.9 (0.92)	2.5	0.55	3.4	0.56	0.070
248 [5.00]	0.45	0.93	>0	0.77	0.015	-
308 [4.02]	0.40	>0	>0	0.71	-	-
351 [3.53]	>0	-	-	-	-	-

References

1 G. M. Muñoz Caro and W. A. Schutte, *Astron. & Astrophys.*, 2003, **412**, 121–132.

2 K. I. Öberg, R. T. Garrod, E. F. van Dishoeck and H. Linnartz, *Astron. & Astrophys.*, 2009, **504**, 891–913.

3 K. I. Öberg, E. F. van Dishoeck, H. Linnartz and S. Andersson, *Astrophys. J.*, 2010, **718**, 832–840.

4 N. G. Petrik, R. J. Monckton, S. P. K. Koehler and G. A. Kimmel, *J. Chem. Phys.*, 2014, **140**, 204710.

5 Q.-B. Lu, *Phys. Rep.*, 2010, **487**, 141–167.

6 A. Bumajdad and M. Madkour, *Phys. Chem. Chem. Phys.*, 2014, **16**, 7146.

7 B. C. Garrett, D. A. Dixon, D. M. Camaioni, D. M. Chipman, M. A. Johnson, C. D. Jonah, G. A. Kimmel, J. H. Miller, T. N. Rescigno, P. J. Rossky, S. S. Xantheas, S. D. Colson, A. H. Laufer, D. Ray, P. F. Barbara, D. M. Bartels, K. H. Becker, H. Bowen, S. E. Bradforth, I. Carmichael, J. V. Coe, L. R. Corrales, J. P. Cowin, M. Dupuis, K. B. Eisenthal, J. A. Franz, M. S. Gutowski, K. D. Jordan, B. D. Kay, J. A. LaVerne, S. V. Lymar, T. E. Madey, C. W. McCurdy, D. Meisel, S. Mukamel, A. R. Nilsson, T. M. Orlando, N. G. Petrik, S. M. Pimblott, J. R. Rustad, G. K. Schenter, S. J. Singer, A. Tokmakoff, L. S. Wang, C. Wittig and T. S. Zwier, *Chem. Rev.*, 2005, **105**, 355–389.

8 Y.-P. Kuo, H.-C. Lu, Y.-J. Wu, B.-M. Cheng and J. F. Ogilvie, *Chem. Phys. Lett.*, 2007, **447**, 168–174.

9 M. Denk, M. Hohage, L. D. Sun, P. Zeppenfeld, N. Esser and C. Cobet, *Surf. Sci.*, 2014, **627**, 16–22.

10 J. Stähler, U. Bovensiepen, M. Meyer and M. Wolf, *Chem. Soc. Rev.*, 2008, **37**, 2180–2190.

11 Q.-B. Lu and L. Sanche, *J. Chem. Phys.*, 2004, **120**, 2434.

12 U. Bovensiepen, C. Gahl, J. Stähler, M. Bockstedte, M. Meyer, F. Baletto, S. Scandolo, X.-Y. Zhu, A. Rubio and M. Wolf, *J. Phys. Chem. C*, 2009, **113**, 979–988.

13 S. Ryu, J. Chang, H. Kwon and S. K. Kim, *J. Am. Chem. Soc.*, 2006, **128**, 3500–3501.

14 M. Bertin, M. Meyer, J. Stähler, C. Gahl, M. Wolf and U. Bovensiepen, *Faraday Discuss.*, 2009, **141**, 293–307.

15 S. H. Liu, A. D. Miller, K. J. Gaffney, S. Garrett-Roe, I. Bezel and C. Harris, *J. Phys. Chem. B*, 2002, **106**, 12908–12915.

16 A. D. Miller, I. Bezel, K. J. Gaffney, S. Garrett-Roe, S. H. Liu, P. Szymanski and C. B. Harris, *Science*, 2002, **297**, 1163–1166.

17 J. Zhao, B. Li, K. Onda, M. Feng and H. Petek, *Chem. Rev.*, 2006, **106**, 4402–4427.

18 Y. Tamaki, A. Furube, M. Murai, K. Hara, R. Katoh and M. Tachiya, *J. Am. Chem. Soc.*, 2006, **128**, 416–417.

19 X.-L. Zhou, X.-Y. Zhu and J. M. White, *Surf. Sci. Rep.*, 1991, **13**, 73–220.

20 M. A. Henderson, *Surf. Sci. Rep.*, 2002, **46**, 1–308.

21 A. Hodgson and S. Haq, *Surf. Sci. Rep.*, 2009, **64**, 381–451.

22 M. Bowker and R. J. Madix, *Surf. Sci*, 1980, **95**, 190–206.

23 C. Ammon, A. Bayer, G. Held, B. Richter, T. Schmidt and H.-P. Steinrück, *Surf. Sci.*, 2002, **507**, 845–850.

24 B. L. Maschhoff, M. J. Ledema, M. Kwini and J. P. Cowin, *Surf. Sci.*, 1996, **359**, 253–268.

25 Y. Lilach and M. Asscher, *J. Chem. Phys.*, 2002, **117**, 6730–6737.

26 F. Fournier, H. Dubost, S. Carrez, W. Zheng and B. Bourguignon, *J. Chem. Phys.*, 2005, **123**, 184705.

27 S. K. Jo and J. M. White, *Surf. Sci.*, 1991, **255**, 321–326.

28 E. R. Miller, G. D. Muirhead and E. T. Jensen, *J. Chem. Phys.*, 2013, **138**, 084702.

29 A. J. DeSimone, B. O. Olanrewaju, G. A. Grieves and T. M. Orlando, *J. Chem. Phys.*, 2013, **138**, 084703.

30 Z. J. Sun, A. L. Schwaner and J. M. White, *J. Chem. Phys.*, 1995, **103**, 4279.

31 D. Marinica, D. Teillet-Billy, J. Gauyacq, M. Michaud and L. Sanche, *Phys. Rev. B*, 2001, **64**, 085408.

32 F. Weik, A. de Meijere and E. Hasselbrink, *J. Chem. Phys.*, 1993, **99**, 682–694.

33 T. Gougousi, P. C. Samartzis and T. N. Kitsopoulos, *J. Chem. Phys.*, 1998, **108**, 5742–5746.

34 F. Wang, M. L. Lipciuc, A. Kartakoullis, P. Glodic, P. C. Samartzis, X. Yang and T. N. Kitsopoulos, *Phys. Chem. Chem. Phys.*, 2014, **16**, 599–606.

35 D. Townsend, S. K. Lee and A. G. Suits, *J. Phys. Chem. A*, 2004, **108**, 8106–8114.

36 F. M. Zimmermann and W. Ho, *Surf. Sci. Rep.*, 1995, **22**, 127–247.

37 X.-L. Zhou and J. M. White, in *Laser Spectroscopy and Photochemistry on Metal Surfaces: Part II*, ed. H.-L. Dai and W. Ho, World Scientific, 1995, ch. Photodissociation and Photoreaction of Molecules Attached to

Metal Surfaces, p. 1173.

38 E. T. Jensen, *J. Chem. Phys.*, 2005, **123**, 204709.

39 G. L. Fisher and C. A. Meserole, *J. Vac. Sci. Tech. A*, 2005, **23**, 722–724.

40 A. Peremans, F. Maseri, J. Darville and J.-M. Gilles, *J. Vac. Sci. Tech. A*, 1990, **8**, 3224–3228.

41 P.-T. Howe and H.-L. Dai, *J. Chem. Phys.*, 1998, **108**, 7775–7782.

42 T. L. Gilton, C. P. Dehnbostel and J. P. Cowin, *J. Chem. Phys.*, 1989, **91**, 1937–1938.

43 S. K. Jo and J. M. White, *J. Chem. Phys.*, 1991, **94**, 5761–5764.

44 *CRC Handbook of Chemistry and Physics*, ed. D. R. Lide, Taylor and Francis, 94th edn, 2013-14.

45 P. Ayotte, J. Gamache, A. D. Bass, I. Fabrikant and L. Sanche, *J. Chem. Phys.*, 1997, **106**, 749–713.

46 M. Michaud and L. Sanche, *J. Elec. Spectrosc. Relat. Phenom.*, 1990, **51**, 237–248.

47 V. A. Ukraintsev, T. J. Long, T. Gowl and I. Harrison, *J. Chem. Phys.*, 1992, **96**, 9114–9123.

48 V. A. Ukraintsev, T. J. Long and I. Harrison, *J. Chem. Phys.*, 1992, **96**, 3957.

49 H. Keller-Rudek, G. K. Moortgat, R. Sander and R. Sörensen, *Earth Syst. Sci. Data*, 2013, **5**, 365–373.

50 D. Lackey, J. Schott, B. Straehler and J. K. Sasss, *J. Chem. Phys.*, 1989, **91**, 1365–1376.

51 H. Petek, *J. Chem. Phys.*, 2012, **137**, 091704.

52 E. T. Jensen, *J. Chem. Phys.*, 2008, **128**, 044301.

53 Y. Lilach and M. Asscher, *J. Chem. Phys.*, 2003, **119**, 407–406.

54 R. D. Burbank, *J. Am. Chem. Soc.*, 1953, **75**, 1211–1214.

55 T. Kawaguchi, M. Hijikigawa, Y. Hayafuji, M. Ikeda, R. Fukushima and Y. Tomiie, *Bull. Chem. Soc. Japan*, 1973, **46**, 53–56.

56 S. Jørgensen, F. Dubnikova, R. Kosloff, Y. Zeiri, Y. Lilach and M. Asscher, *J. Phys. Chem. B*, 2004, **108**, 14056–14061.

57 S. J. Dixon-Warren, D. V. Heyd, E. T. Jensen and J. C. Polanyi, *J. Chem. Phys.*, 1993, **98**, 5954.

58 X.-L. Zhou, F. Solymosi, P. M. Blass, K. C. Cannon and J. M. White, *Surf. Sci*, 1989, **219**, 294–316.

59 A. Yamakata, T. Ishibashi and H. Onishi, *J. Phys. Chem. B*, 2002, **106**, 9122–9125.

60 T. Rander, A. Lindblad, I. Bradeanu, G. Öhrwall, S. Svensson and O. Björneholm, *J. Chem. Phys.*, 2014, **141**, 224305.